

Supporting Information

An Easily Synthesized Microporous Framework Material for the Selective Capture of Radioactive Cs⁺ and Sr²⁺ Ions

Yu-Jie Gao,^{a, b} Mei-Ling Feng*,^a Bo Zhang,^a Zhao-Feng Wu,^a Ying Song,^a and Xiao-Ying Huang*^a

^aState Key Laboratory of Structural Chemistry, Fujian Institute of Research on the Structure of Matter, Chinese Academy of Sciences, Fuzhou, Fujian 350002, P. R. China

^bCollege of Chemistry, Fuzhou University, Fuzhou, Fujian 350002, P. R. China

- 1. Experimental section**
- 2. More crystal structures details**
- 3. Characterization of products before and after ion exchange**
- 4. Kinetic studies of ion exchange**
- 5. The ion-exchange capacity**
- 6. The studies on competitive ion exchange**
- 7. The elution**
- 8. The studies on the stability of FJSM-InMOF**

1. Experimental section



Figure S1. (a) Gram-scale synthesis of FJSM-InMOF (there are about 15 g as-made crystalline products in the vial). (b) Photo of the air-dried crystalline products without washing or manual selection.

Physical Measurements

Element analyses (EA) of C, H, and N were measured by a German Elementary Vario EL III instrument. Energy-dispersive spectroscopy (EDS) and Scanning electron microscope (SEM) analyses were performed with a JEOL JSM-6700F scanning electron microscope and HITACHI FE-SEM SU8010, respectively. UV/Vis spectra were collected by using BaSO_4 as a standard (100% reflectance) at room temperature with a Shimadzu 2600 UV/Vis spectrometer. Emission and excitation spectra of the products were recorded on a PerkinElmer LS55 luminescence spectrometer. Thermogravimetric (TG) analyses were carried out with a NETZSCH STA 449F3 unit at a heating rate of $10\text{ }^\circ\text{C}/\text{min}$ under a nitrogen atmosphere. Powder X-ray diffraction (PXRD) patterns were performed with a Miniflex II diffractometer at 30 kV and 15 mA using $\text{CuK}\alpha$ (1.54178 \AA) in the angular range of $2\theta = 5\text{-}55^\circ$ at room temperature. The simulated PXRD patterns through single crystal data were generated by using the Mercury program. γ irradiation was conducted using a ^{60}Co irradiation source (60000 curie). The sample FJSM-InMOF was irradiated at a dose rate of $1.2\text{ kGy}/\text{h}$ for three different doses of 20, 100 and 200 kGy in γ irradiation experiment. β irradiation was conducted using electron beams (1.2 MeV) which were provided by an electron accelerator. The sample was irradiated at a dose rate of $20\text{ kGy}/\text{h}$ for three different doses of 20, 80 and 100 kGy. Gas adsorption measurement was performed in an ASAP (Accelerated Surface Area and Porosimetry) 2020 System. X-ray photoelectron spectroscopy (XPS) was carried out on an ESCALAB 250Xi X-ray Photoelectron Spectrometer Microprobe. Inductively coupled plasma-optical emission spectroscopy (ICP-OES) was performed on a Thermo 7400. Inductively coupled plasma-mass spectroscopy (ICP-MS) was carried on a XSeries II.

Single-crystal X-ray diffraction data for FJSM-InMOF and FJSM-InMOF-Cs were collected on a SuperNova CCD diffractometer with graphite-monochromated $\text{MoK}\alpha$ (0.71073 \AA) at $100(2)\text{ K}$. The structures were solved by direct methods and refined by full-matrix least-squares on F^2 by using the program SHELX-2016. In FJSM-InMOF, both the crystallographic independent one and a half of DMA molecule are disordered over two positions with refined S.O.F. ratios of $0.631(10)/0.369(10)$ and $0.226(12)/0.274(12)$, respectively. While the guest water

molecules are highly disordered thus the H atoms attached to the water oxygen atoms were not added. However, the empirical formula was confirmed by the TGA (Figure S9) and EA results. In FJSM-InMOF-Cs, since the guest water and CH₃OH molecules are highly disordered and only some of the water molecules could be found from the difference-Fourier maps, a Squeeze process was applied before the final structural refinement. However, the empirical formula was confirmed by the TGA (Figure S9) and EA results (For CsIn(TDC)₂·1.5H₂O·0.25MeOH: found, C, 23.47%; H, 1.34%; N, ≤0.03%; calculated: C, 23.61%; H, 1.30%; N, 0%). The crystallographic data and structural refinement details for FJSM-InMOF and FJSM-InMOF-Cs are listed in Table S1. The selected bond distances and hydrogen bonding information for FJSM-InMOF are listed in Tables S2 and S3, respectively. In order to see how the Cs atoms were surrounded by the guest solvent molecules, we also tried locating the disordered water molecules to the structural model; the Cs-O distances are listed in Table S4. CCDC 1561632 for FJSM-InMOF and 1561634 for FJSM-InMOF-Cs contain the supplementary crystallographic data for this paper.

The product after Sr²⁺ ion exchange was denoted as FJSM-InMOF-Sr. The cell parameters for FJSM-InMOF-Sr were determined on a SuperNova CCD diffractometer with graphite-monochromated MoK α (0.71073 Å) at 100(2) K as follows: $a = b = 13.514(9)$ Å, $c = 15.486(11)$ Å, $\alpha = \beta = \gamma = 90^\circ$, $V = 2828(3)$ Å³. However, good-quality single-crystal X-ray intensity data could not be obtained to reveal the crystal structural details of FJSM-InMOF-Sr due to poor quality of the single crystal. While the similar phenomenon of single-crystal to single-crystal structural transformation as that in the Cs⁺-exchange process has been evidenced both from the differences of unit cell parameters of the single-crystals before and after Sr²⁺-exchange and the PXRD pattern deposited in Figure S11a.

Ion-exchange Experiments

Considering the high toxicity of ¹³⁷Cs and ⁹⁰Sr, the ion exchange experiments were carried out using the solution of their nonradioactive isotopes. To a methanol solution of CsCl or SrCl₂ with the different concentrations of Cs⁺ or Sr²⁺ ions (15 mL), the ground polycrystalline powders of FJSM-InMOF (15 mg) were added. The mixture was kept under magnetic stirring at room temperature (~ 25°C). Then the yellow polycrystalline material was separated by filtration and washed several times with methanol. The concentrations of Cs⁺ and Sr²⁺ in the clear supernatant, which has been filtered by the 0.22 μm Millipore filter on the 10 mL syringe and diluted with ultrapure water to meet the concentration range of the test instrument, were determined by plasma-optical emission spectroscopy (ICP-OES) or inductively coupled plasma-mass spectroscopy (ICP-MS).

The kinetic studies of Cs⁺ and Sr²⁺ ion-exchange by FJSM-InMOF were done by carrying out ion-exchange experiments with various reaction times. 250 mg of FJSM-InMOF polycrystalline powders were weighed into a 100 mL sample of methanol solution containing 90.7 ppm of Cs⁺ or 17.4 ppm of Sr²⁺, and the mixtures were kept under magnetic stirring at the various reaction times. The suspensions after filtering and diluting were analyzed by inductively coupled plasma-mass spectroscopy (ICP-MS) (Tables S5 and S6).

In the isotherm experiments, the solutions of Cs⁺ and Sr²⁺ with different concentrations were prepared, respectively. The V/m of all the samples is 1000 mL/g ($V = 15$ mL, $m = 15$ mg). The ion-exchange lasted about 12 h for Cs⁺ and 24 h for Sr²⁺ at room temperature (~ 25°C). Then the suspensions after filtering and diluting were

analyzed by inductively coupled plasma-mass spectroscopy (ICP-MS) (Tables S7 and S8) and the samples were taken out and processed.

The competitive ion-exchange experiments of Cs⁺ and Sr²⁺ by FJSM-InMOF in the presence of individual alkali or alkaline-earth metal ions, such as K⁺, Na⁺, Rb⁺, Ca²⁺ and Mg²⁺ (Tables S9 and S10) were carried out at *V/m* ratios of 1000 mL/g, room temperature (~ 25°C), 12 h contact time for Cs⁺ and 24 h contact time for Sr²⁺. Especially, ion-exchange experiments in the presence of NaCl (NaCl:Cs molar ratios were in the range of 26.56–2.00 × 10⁴) (Tables S11 and S13) and NaNO₃ (NaNO₃:Cs molar ratios were in the range of 23.87–1.91 × 10⁴) (Tables S12 and S14) were carried out at *V/m* ratio of 1000 mL/g or 100 mL/g, room temperature (~ 25°C), and 12 h contact time. In the competitive experiments with mixed metal ions, the selective ion exchange of FJSM-InMOF for Cs⁺ or Sr²⁺ were investigated at *V/m* ratio of 1000, 200 or 100 mL/g, room temperature (~ 25°C), 12 h contact time for Cs⁺ and 24 h contact time for Sr²⁺ (Table S15). Finally, the individual Cs⁺ or Sr²⁺ ion exchange experiment were carried out at *V/m* ratio of 1000 mL/g, room temperature (~ 25°C), 12 h contact time for Cs⁺ and 24 h contact time for Sr²⁺, in which the initial concentrations of Cs⁺ and Sr²⁺ ions are 679.6 ppb and 1240 ppb, respectively (Table S16). The ion exchange ability of FJSM-InMOF in the methanol solutions with the coexistence of 1176 ppb Cs⁺ and 1140 ppb Sr²⁺ was also studied at *V/m* ratio of 1000 mL/g, room temperature (~ 25°C), 24 h contact time (Table S16).

In order to elute the materials, Cs⁺-exchanged products of ~25 mg were used in the elution experiments by applying 50 mL saturated KCl methanol solution (~1300 ppm) under magnetic stirring for 4 days at room temperature (~ 25°C). After this treatment, the solid samples were analyzed with the EDS and PXRD measurements.

2. More Crystal structures details

Table S1. Crystallographic data and structural refinement details for FJSM-InMOF and FJSM-InMOF-Cs.

	FJSM-InMOF	FJSM-InMOF-Cs
Empirical formula	C ₂₀ H _{28.50} InN _{2.50} O ₁₁ S ₂	C _{12.25} H ₈ CsInO _{9.75} S ₂
Formula weight	658.89	623.04
Temperature/K	100(2)	100(2)
Wavelength/Å	0.71073	0.71073
Crystal system	orthorhombic	tetragonal
space group	<i>Pccn</i>	<i>P4₁22</i>
<i>a</i> /Å	14.9001(5)	13.6387(5)
<i>b</i> /Å	19.3837(6)	13.6387(6)
<i>c</i> /Å	19.5935(6)	15.1597(6)
<i>V</i> / Å ³	5659.0(3)	2819.9(4)
<i>Z</i>	8	4
<i>D</i> _{calc.} (mg/m ³)	1.547	1.468
F(000)	2680	1182
Crystal size (mm ³)	0.22 × 0.16 × 0.14	0.20 × 0.12 × 0.10
Theta range for data collection	3.437 to 28.517	3.601 to 28.818
Limiting indices	-19<= <i>h</i> <=15, -23<= <i>k</i> <=21, -26<= <i>l</i> <=25	-18<= <i>h</i> <=15, -18<= <i>k</i> <=14, -15<= <i>l</i> <=20

Completeness to theta = 25.242	99.7 %	99.3 %
Refinement method	Full-matrix least-squares on F^2	Full-matrix least-squares on F^2
Data / restraints / parameters	6213 / 887 / 495	3295 / 15 / 111
Goodness-of-fit on F^2	1.062	1.038
Final R indices [$I > 2\sigma(I)$]	$R_1 = 0.0635$, $wR_2 = 0.1592$	$R_1 = 0.0930$, $wR_2 = 0.2028$
R indices (all data)	$R_1 = 0.0740$, $wR_2 = 0.1672$	$R_1 = 0.1424$, $wR_2 = 0.2321$
CCDC	1561632	1561634

[a] $R_1 = \frac{\sum \|F_o\| - \|F_c\|}{\sum \|F_o\|}$, $wR_2 = \frac{[\sum w(F_o^2 - F_c^2)^2 / \sum w(F_o^2)^2]^{1/2}}$.

Table S2. Selected bond lengths (Å) of FJSM-InMOF.

In(1)-O(8) ⁱ	2.166(5)
In(1)-O(2)	2.190(4)
In(1)-O(4) ⁱⁱ	2.200(4)
In(1)-O(6)	2.220(4)
In(1)-O(5)	2.297(4)
In(1)-O(1)	2.376(4)
In(1)-O(3) ⁱⁱⁱ	2.389(4)
In(1)-O(7) ⁱ	2.477(5)

Symmetry transformations used to generate equivalent atoms:

i $-x+3/2, y, z+1/2$; ii $-x+1, y-1/2, -z+3/2$.

Table S3. Selected hydrogen bonds of FJSM-InMOF.

D-H...A	d(D-H)	d(H...A)	d(D...A)	<(DHA)
N(1)-H(1A)···O(2) ⁱ	0.91	2.47	3.126(9)	129.4
N(1)-H(1A)···O(3)	0.91	2.23	2.949(9)	136.0
N(1)-H(1A)···O(7) ⁱⁱ	0.91	2.28	2.973(10)	132.6
N(1)-H(1B)···O(2W)	0.91	1.91	2.752(14)	152.3

Symmetry transformations used to generate equivalent atoms:

i $-x+1, y+1/2, -z+3/2$; ii $x-1/2, y+1/2, -z+1$.

Table S4. Selected bond lengths (Å) of FJSM-InMOF-Cs.

Cs(1)-O(2)	3.041(16)
Cs(1)-O(2) ⁱ	3.041(16)
Cs(1)-O(3) ⁱⁱ	3.156(15)
Cs(1)-O(3) ⁱⁱⁱ	3.156(15)
Cs(1)-O(1W)	3.19(5)
Cs(1)-O(1W) ⁱ	3.19(5)
Cs(1)-O(3W) ⁱ	3.33(10)
Cs(1)-O(3W)	3.33(10)
Cs(1)-O(2W)	3.375(4)
In(1)-O(1) ^{iv}	2.21(2)
In(1)-O(1)	2.21(2)
In(1)-O(3) ^v	2.232(15)

In(1)-O(3) ⁱⁱⁱ	2.232(15)
In(1)-O(2) ^{iv}	2.316(17)
In(1)-O(2)	2.316(17)
In(1)-O(4) ^v	2.345(14)
In(1)-O(4) ⁱⁱⁱ	2.345(14)

Symmetry transformations used to generate equivalent atoms:

i $-x+1, y, -z$; ii $y, -x, z-1/4$; iii $-y+1, -x, -z+1/4$; iv $x, -y, -z+1/2$; v $-y+1, x, z+1/4$.

Figure S2 show the asymmetric units for FJSM-INMOF and FJSM-InMOF-Cs. More structural details are depicted in Figures S3-S8. In FJSM-InMOF, In^{3+} is coordinated by eight oxygen atoms from four TDC²⁻ ligands via a bidentate chelating fashion to form a trigonal dodecahedral $[\text{InO}_8]$ polyhedron. Two TDC ligands adopt the same coordination mode and bridge two In^{3+} ions via bidentate chelating COO^- groups, respectively (Figure S3a).

The asymmetric unit of FJSM-InMOF-Cs contains half a formula unit (Figure S2a). The TDC²⁻ ligand bridges two In^{3+} ions as that of FJSM-InMOF and also connects two Cs^+ ions via unidentate oxygen atoms with two COO^- groups (Figures S3b). Cs^+ ion is nine-coordinated with five water molecules and four oxygen atoms from four TDC²⁻ ligands with $\text{Cs}-\text{O}$ distances in the range of 3.041(16)–3.375(4) Å (Figures S6 and S7; Table S4).

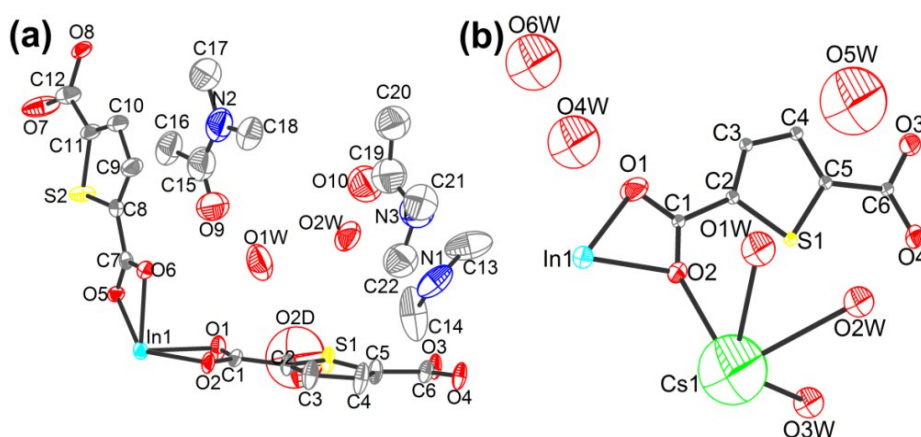


Figure S2. ORTEP plot showing the crystallographically asymmetric units in FJSM-InMOF (a) and FJSM-InMOF-Cs (b). Thermal ellipsoids are given at the 50% probability level. Hydrogen atoms are not shown.

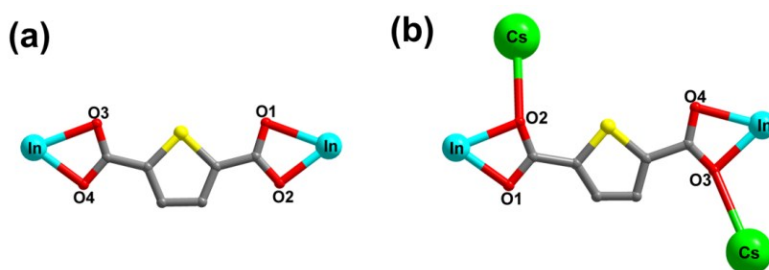


Figure S3. The connection types of TDC ligands in FJSM-InMOF (a) and FJSM-InMOF-Cs (b).

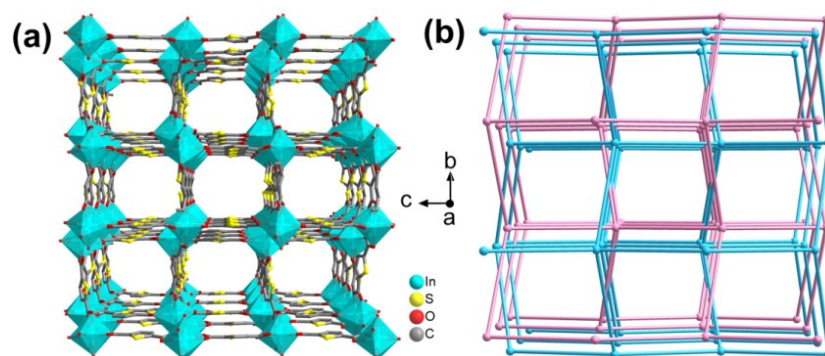


Figure S4. (a) 3D open framework of FJSM-InMOF viewed along the a axis; guest cations and solvent molecules in the channels are omitted for clarity. (b) Two-fold interpenetrating diamond nets of FJSM-InMOF viewed along the a axis.

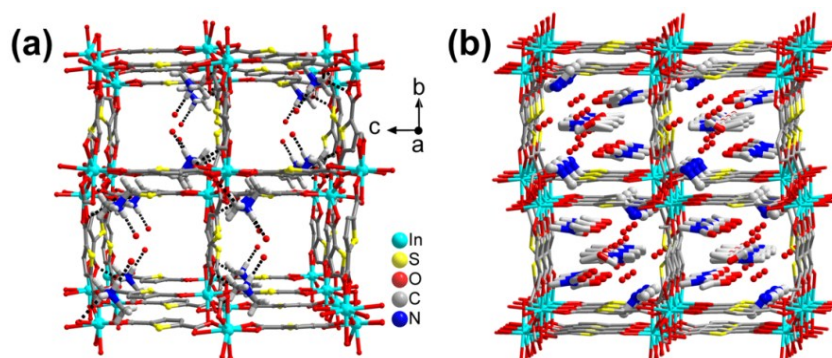


Figure S5. (a) A view along the a axis for the 3D open framework of FJSM-InMOF with hydrogen bonds shown; the lattice water and DMA molecules in the channels are omitted for clarity. (b) 3D open framework of FJSM-InMOF viewed along the a axis with $[\text{Me}_2\text{NH}_2]^+$ cations, the guest of lattice water and DMA molecules in the channels. Hydrogen atoms are omitted for clarity.

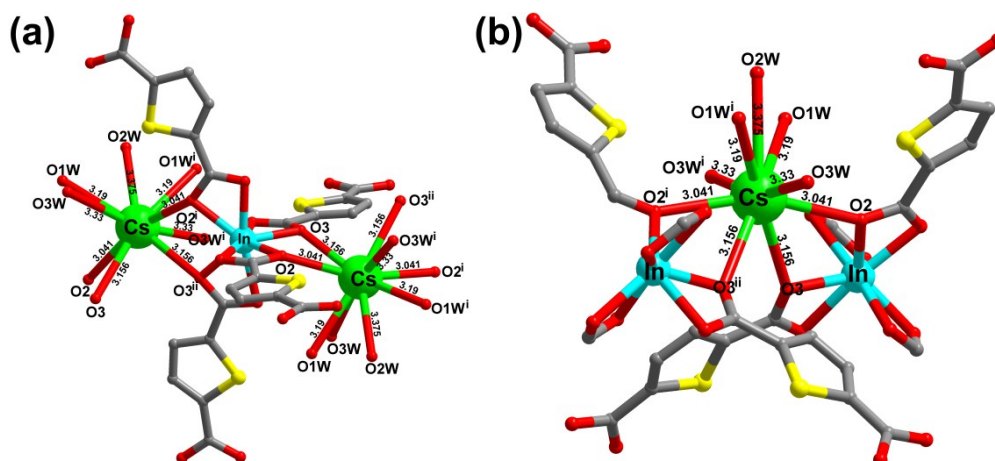


Figure S6. Connection types of In^{3+} ions (a) and Cs^+ ions (b) in FJSM-InMOF-Cs. Symmetry codes: i $-x+1, y, -z$; ii $y, -x, z-1/4$.

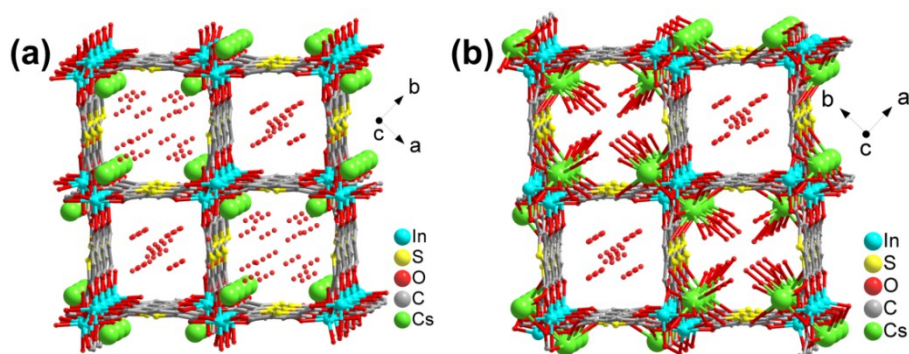


Figure S7. (a) 3D open framework of FJSM-InMOF-Cs along the c axis; the coordination bonds of Cs^+ are omitted for clarity. (b) 3D open frameworks FJSM-InMOF-Cs along the c axis with the coordination bonds of Cs^+ .

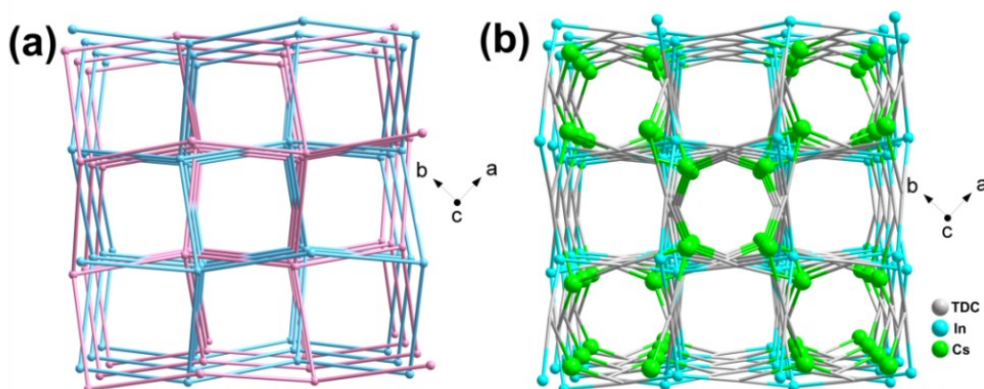


Figure S8. (a) Two-fold interpenetrating diamond nets of $[\text{In}(\text{TDC})_2]_n^{n-}$ in FJSM-InMOF-Cs viewed along the c axis, in which the nodes are In^{3+} ions and TDC^{2-} act as ligands. The Cs^+ ions are omitted in the topology analysis. (b) A neutral PtS topological net of FJSM-InMOF-Cs is formed by two-fold interpenetrating anionic frameworks of $[\text{In}(\text{TDC})_2]_n^{n-}$ weaved by Cs^+ ions viewed along the c axis; the nodes are In^{3+} , Cs^+ ions and TDC^{2-} act as ligands.

3. Characterization of products before and after ion exchange

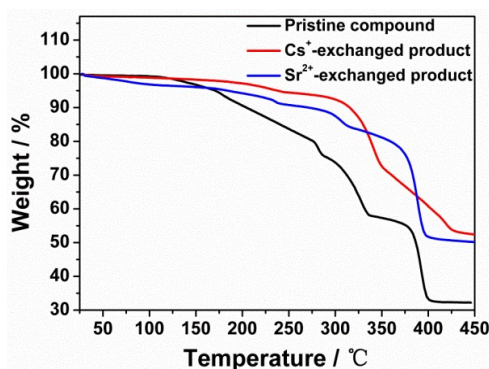


Figure S9. TGA curves for the pristine compound, Cs^+ -exchanged product (initial Cs^+ concentration of 2000 ppm, $V : m = 1000 \text{ mL g}^{-1}$, contact time 8 h and room temperature $\sim 25^\circ\text{C}$) and Sr^{2+} -exchanged product (initial Sr^{2+} concentration of 1500 ppm, $V : m = 1000 \text{ mL g}^{-1}$, contact time 24 h and room temperature $\sim 25^\circ\text{C}$).

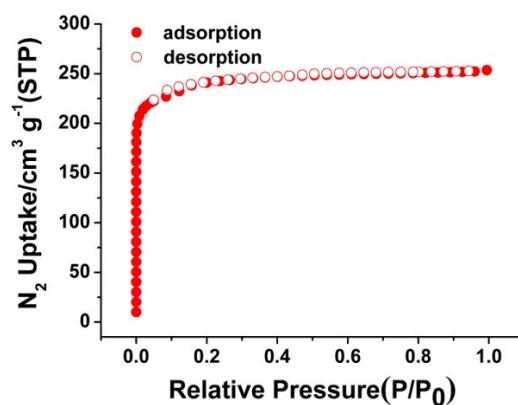


Figure S10. The N_2 sorption isotherm for the activated FJSM-InMOF at 77 K.

The measurement for the BET surface area of FJSM-InMOF was conducted at 77 K with a liquid nitrogen bath and the detecting pressures ranging from 0 to 760 Torr. Before adsorption measurement, the sample was activated using the “degass” function of the surface area analyser at 170°C for 11 h.

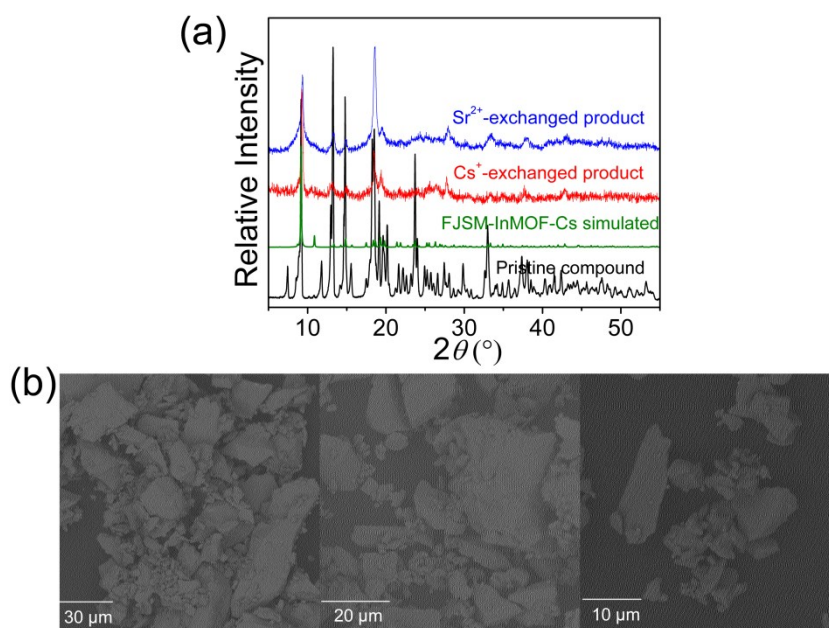
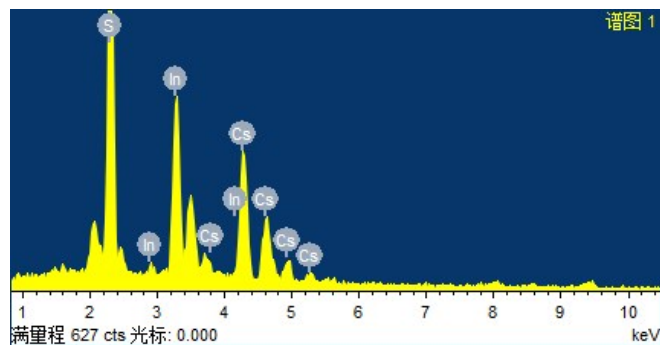
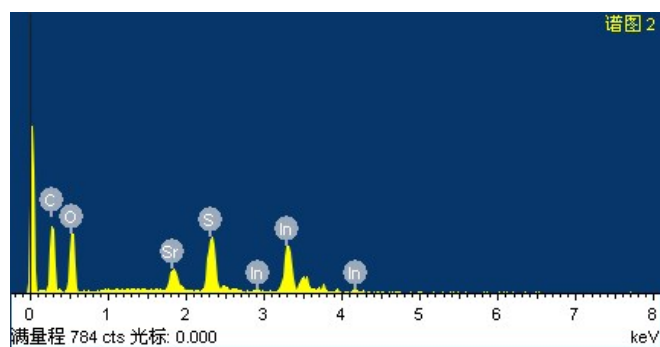


Figure S11. (a) PXRD patterns of pristine compound, simulated FJSM-InMOF-Cs, and Cs^+ and Sr^{2+} -exchanged products. The Cs^+ and Sr^{2+} -exchanged products are the samples of the highest concentration in the cesium and strontium adsorption isotherm models, respectively. (b) SEM images for the FJSM-InMOF polycrystalline powders that were used in adsorption isotherm, kinetics and competitive ion exchange experiments, showing the particle size is in the tens micrometers magnitude.



Element	Weight percentage	Atom percentage
S K	21.72	51.74
In L	36.09	24.01
Cs L	42.19	24.25
Total	100.00	

Figure S12. EDS diagram and data for one of the Cs⁺-exchanged products. The results show that the ratio of In/Cs = 0.99 : 1 approaches the theoretical ratio of 1 : 1. ($V : m = 1000 \text{ mL g}^{-1}$, contact time 24 h, room temperature $\sim 25^\circ\text{C}$, and initial Cs⁺ concentration of 2000 ppm).



Element	Weight percentage	Atom percentage
S K	18.64	43.55
In L	64.43	42.00
Sr L	16.93	14.45
Total	100.00	

Figure S13. EDS diagram and data for one of the Sr²⁺-exchanged products. The results show that the ratio of In/Sr = 2.91 : 1 is larger than the theoretical ratio of 2 : 1 which further verifies that the practical ion-exchange capacity is about 66% of the theoretical value. ($V/m = 1000 \text{ mL g}^{-1}$, contact time 24 h, room temperature $\sim 25^\circ\text{C}$, and initial Sr²⁺ concentration of 1500 ppm).

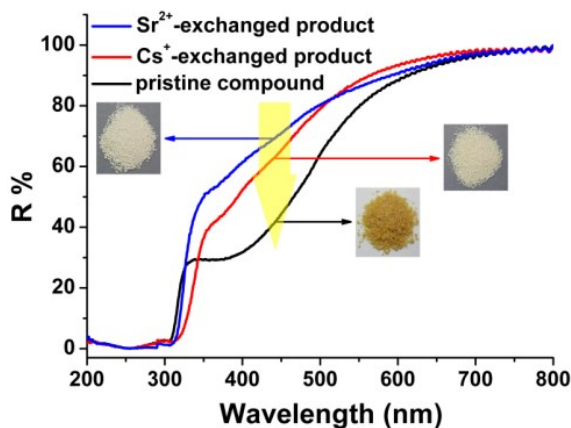


Figure S14. UV-Vis diffuse reflectance spectra of pristine compound, and Cs⁺ and Sr²⁺-exchanged products ($V/m = 1000$ mL/g, contact time 24 h, room temperature $\sim 25^\circ\text{C}$, initial Cs⁺ and Sr²⁺ concentrations are ~ 2000 ppm and ~ 1500 ppm, respectively).

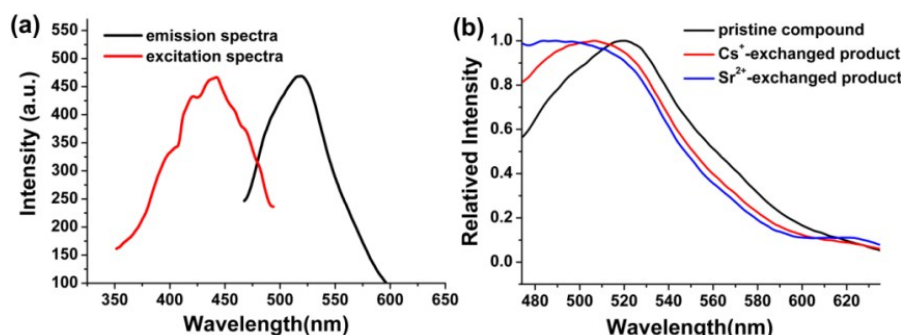


Figure S15. (a) Solid state excitation and emission spectra of FJSM-InMOF ($\lambda_{ex} = 442$ nm, $\lambda_{em} = 520$ nm). (b) Emission spectra of the pristine compound and Cs⁺ and Sr²⁺-exchanged products ($\lambda_{ex} = 442$ nm).

The strongest absorption band of FJSM-InMOF is around 442 nm which has been demonstrated in the solid-state photoluminescence (Figure S15a). The absorption bands of the Cs⁺ and Sr²⁺-exchanged products become weaker compared with the pristine compound (Figure S14). And accordingly, triggering by the same excitation wavelength the emission spectra of the Cs⁺ and Sr²⁺-exchanged products exhibit a significant blue shift compared to the pristine compound (Figure S15b). The weaker absorption band is consistent with the lighter colors of the Cs⁺ and Sr²⁺-exchanged products (Figure S14).

4. Kinetic studies of ion exchange

Table S5. The data for the concentrations of cesium (C_i) and the relative amounts of Cs⁺ removed (R) at the different time in kinetics experiments.

Time (minutes)	C_i (ppm)	R (%)
0	90.7	0
5	51.6	43.10915
10	46.2	49.06284
20	32.6	64.05733
30	24.8	72.65711

60	15.4	83.02095
120	9.2	89.85667
180	7.5	91.73098
300	6.1	93.27453
1320	4.3	95.25910

Table S6. The data for the concentrations of strontium (C_t) and the relative amounts of Sr^{2+} removed (R) at the different time in kinetics experiments.

Time (minutes)	C_t (ppm)	R (%)
0	17.4	0
11	13	25.28736
21	10.6	39.08046
60	8.1	53.44828
120	7.2	58.62069
180	6.3	63.7931
360	5.8	66.66667
480	5.6	67.81609
600	5.3	69.54023
720	4.8	72.41379
1320	4.4	74.71264
2040	3.5	79.88506
2160	3.5	79.88506

5. The ion-exchange capacity

Table S7. Exchange capacities for isotherm studies at the different initial Cs^+ concentrations.

Cs concentration (ppm)	Cs concentration (ppm)	q (mg/g)
C_0	C_e	
27	12	15
82	18	64
232	90	142
280	132	148
550	380	170
760	580	180
940	750	190

Table S8. Exchange capacities for isotherm studies at the different initial Sr^{2+} concentrations.

Sr^{2+} concentration (ppm)	Sr^{2+} concentration (ppm)	q (mg/g)
C_0	C_e	
21.2	11.52	9.68
50.6	32.8	17.8
121.8	93.2	28.6
160	126	34
234.2	199.2	35
261	224.2	36.8
530	490	40

The theoretical ion-exchange capacity:

The theoretical ion-exchange capacity means Cs⁺ and Sr²⁺ adsorption capacity of FJSM-InMOF [Me₂NH₂][In(TDC)₂].1.5DMA.1.5H₂O when all organic amine cations in FJSM-InMOF are completely exchanged by cesium or strontium. According to molecule formula of FJSM-InMOF, theoretically each molecule of FJSM-InMOF can capture one Cs⁺ cation or a half of Sr²⁺ cation. Here, the theoretical ion-exchange capacity q (mg·g⁻¹) for Cs⁺ and Sr²⁺ of FJSM-InMOF can be calculated from the equations S1 and S2, respectively.

$$q(\text{theoretical}) = \frac{\text{Atomic weight of cesium}}{\text{Formula weight of FJSM - InMOF}} \times 1000 = \frac{132.90}{658.89} \times 1000 = 201.70 \text{ mg}\cdot\text{g}^{-1}$$

(Equation S1)

$$q(\text{theoretical}) = \frac{\text{Half of atomic weight of strontium}}{\text{Formula weight of FJSM - InMOF}} \times 1000 = \frac{0.5 \times 87.62}{658.89} \times 1000 = 66.35 \text{ mg}\cdot\text{g}^{-1}$$

6. The studies on competitive ion exchange

a. The Cs⁺ and Sr²⁺ competitive ion exchange with individual competitive alkali or alkaline-earth ions.

Table S9. The results for the Cs⁺-exchange of FJSM-InMOF with individual competitive alkali or alkaline-earth ions ($V/m = 1000$ mL/g, room temperature ~ 25°C, 12 h contact time).

Competing cation	Cs/K	Cs/Na	Cs/Rb	Cs/Ca	Cs/Mg
Molar ratio	6.506	23.87	12.048	14.517	9.144
Cs (ppb) C_0	647.8	760.4	752.4	662.4	681.6
Cs (ppb) C_e	13.6	10	16.6	23	14.8
% Cs Removal	97.90	98.69	97.79	96.53	97.83
K_d^{Cs} (mL/g)	4.66×10^4	7.50×10^4	4.43×10^4	2.78×10^4	4.51×10^4
M (ppb) C_0	1240	3140	5830	2900	1140
M (ppb) C_e	460	2740	304	1360	460
% M Removal	62.90	12.74	94.79	53.10	59.65
K_d^{M} (mL/g)	1.70×10^3	1.46×10^2	1.82×10^4	1.13×10^3	1.48×10^3
SF	27.50	514.02	2.44	24.55	30.48

Table S10. The results for the Sr²⁺-exchange of FJSM-InMOF with individual competitive alkali or alkaline-earth M ions ($V/m = 1000$ mL/g, room temperature ~ 25°C, 24 h contact time).

Competing cation	Sr/K	Sr/Na	Sr/Rb	Sr/Ca	Sr/Mg
Molar ratio	5.86	22.23	5.58	9.54	15.25
Sr (ppb) C_0	1200	1200	1260	880	1300

Sr (ppb) C_e	18.6	11	26.2	83.2	296.2
% Sr Removal	98.45	99.08	97.92	90.55	77.22
K_d^{Sr} (mL/g)	6.35×10^4	1.08×10^5	4.71×10^4	9.58×10^3	3.39×10^3
M (ppm) C_0	3.14	7	6.854	3.84	5.5
M (ppm) C_e	0.32	5.24	0.4034	1.3	3.2
% M Removal	89.81	25.14	94.11	66.15	41.82
K_d^M (mL/g)	8.81×10^3	3.36×10^2	1.60×10^4	1.95×10^3	7.19×10^2
SF	7.21	321.82	2.94	4.90	4.72

b. The Cs⁺ competitive ion exchange in the presence of large excess NaCl and NaNO₃.

Table S11. The results for the Cs⁺-exchange of FJSM-InMOF with competitive excess Na⁺ ions from NaCl ($V/m = 1000$ mL/g).

Initial Na/Cs molar ratio	V/m (mL/g)	Na	Na	Cs	Cs	R (%)	K_d^{Cs} (mL/g)	K_d^{Na} (mL/g)	SF
		(ppm) C_0	(ppm) C_e	(ppb) C_0	(ppb) C_e				
26.56	1000	3.46	2.64	753	13	98.27	5.69×10^4	3.11×10^2	183.26
176.09	1000	23.4	19.48	768.2	32	95.83	2.30×10^4	2.01×10^2	114.33
1347.08	1000	203.2	186	872	130.2	85.07	5.70×10^3	92.47	61.61
8134.97	1000	194.2	189.8	138	21	84.78	5.57×10^3	23.18	240.33
20045.02	1000	213.6	195.2	61.6	8.2	86.69	6.51×10^3	94.26	69.09

Table S12. The results for the Cs⁺-exchange of FJSM-InMOF with competitive excess Na⁺ ions from NaNO₃ ($V/m = 1000$ mL/g).

Initial Na/Cs molar ratio	V/m (mL/g)	Na	Na	Cs	Cs	R (%)	K_d^{Cs} (mL/g)	K_d^{Na} (mL/g)	SF
		(ppm) C_0	(ppm) C_e	(ppb) C_0	(ppb) C_e				
23.87	1000	3.14	2.74	760.4	10	98.69	7.50×10^4	1.46×10^2	514.02
147.86	1000	18.8	16.28	735	28.4	96.14	2.49×10^4	1.55×10^2	160.73
1529.02	1000	197	184	744.8	114	84.69	5.53×10^3	70.65	78.32
7728.31	1000	200	182.2	149.6	19.6	86.90	6.63×10^3	97.69	67.89
19067.08	1000	201.2	183.8	61	14.6	76.07	3.18×10^3	94.67	33.57

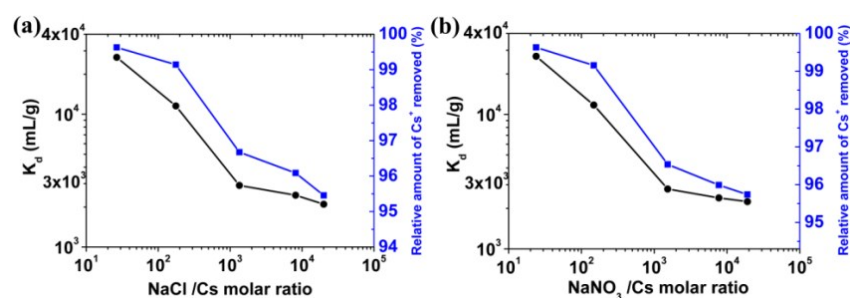


Figure S16. Variations of the distribution coefficient K_d values of Cs⁺ (black line) and the relative amounts of Cs⁺ removed (blue line) with the NaCl/Cs (a) and NaNO₃/Cs (b) molar ratios ($V/m = 100$ mL/g, room temperature $\sim 25^\circ\text{C}$, 12 h contact time).

Table S13. The results for the Cs⁺-exchange of FJSM-InMOF with competitive Na⁺ ions from NaCl ($V/m = 100$ mL/g, room temperature $\sim 25^\circ\text{C}$, 12 h contact time).

Initial Na/Cs molar ratio	V/m (mL/g)	Na (ppm) C_0	Na (ppm) C_e	Cs (ppb) C_0	Cs (ppb) C_e	R (%)	K_d^{Cs} (mL/g)	K_d^{Na} (mL/g)	SF
26.56	100	3.46	2.04	753	2.8	99.63	2.68×10^4	69.61	384.91
176.09	100	23.4	11.1	768.2	6.6	99.14	1.15×10^4	1.11×10^2	104.14
1347.08	100	203.2	145	872	29	96.67	2.91×10^3	40.14	72.42
8134.97	100	194.2	143.8	138	5.4	96.09	2.46×10^3	35.05	70.06
20045.02	100	213.6	157	61.6	2.8	95.46	2.10×10^3	36.05	58.25

Table S14. The results for the Cs⁺-exchange of FJSM-InMOF with competitive Na⁺ ions from NaNO₃ ($V/m = 100$ mL/g, room temperature $\sim 25^\circ\text{C}$, 12 h contact time).

Initial Na/Cs molar ratio	V/m (mL/g)	Na (ppm) C_0	Na (ppm) C_e	Cs (ppb) C_0	Cs (ppb) C_e	R (%)	K_d^{Cs} (mL/g)	K_d^{Na} (mL/g)	SF
23.87	100	3.14	2.06	760.4	2.8	99.63	2.71×10^4	52.43	516.09
147.86	100	18.8	9.74	735	6.2	99.16	1.18×10^4	93.02	126.37
1529.02	100	197	144.8	744.8	25.8	96.54	2.79×10^3	36.05	77.30
7728.31	100	200	146.8	149.6	6	95.99	2.39×10^3	36.24	66.04
19067.08	100	201.2	145.2	61	2.6	95.74	2.25×10^3	38.57	58.24

- c. The ion-exchange performances in the presence of various alkali and alkaline-earth ions to test the affinity of FJSM-InMOF for some alkali and alkaline-earth ions.

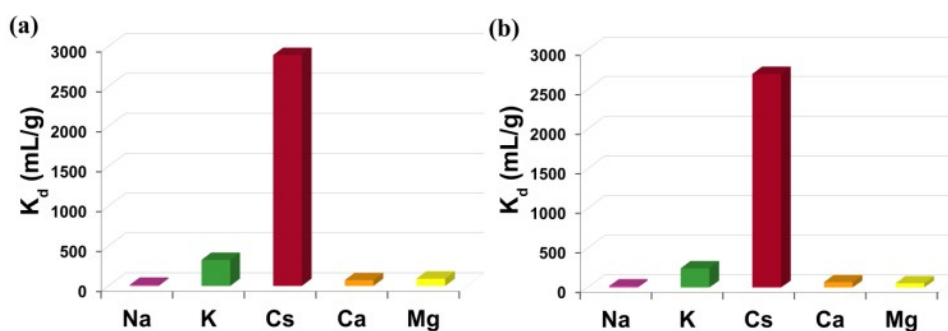


Figure S17. The distribution coefficient K_d values (y axis) of all cations (x axis) in the various metal ions competing experiments. Initial ~ 1.86 ppm of Cs⁺, other alkaline and alkaline-earth cations from 9.18 to 86.9 ppm. (a) $V/m = 200$ mL/g and (b) $V/m = 100$ mL/g, room temperature $\sim 25^\circ\text{C}$, 12 h contact time.

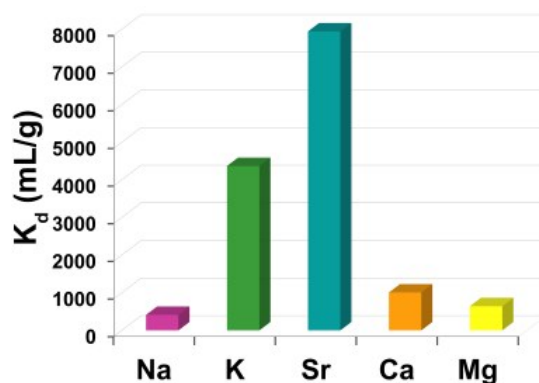


Figure S18. The distribution coefficient K_d values (y axis) of all cations (x axis) in the various metal ions competing experiments. Initial 1.24 ppm of Sr^{2+} , other alkaline and alkaline-earth cations from 4.08 to 12.52 ppm ($V/m = 200$ mL/g, room temperature $\sim 25^\circ\text{C}$, 24 h contact time).

Table S15. The results of ion exchange in the competitive experiments with mixed metal ions. The ion-exchange process for competitive experiments of Cs^+ lasted about 12 h at room temperature ($\sim 25^\circ\text{C}$) and that for competitive experiments of Sr^{2+} lasted about 24 h at room temperature.

Metal cations	Condition	C_0 /ppm	C_e /ppm	R (%)	K_d (mL/g)
$\text{Cs}^+ + \text{Ca}^{2+} + \text{Mg}^{2+} + \text{Na}^+ + \text{K}^+$	$V/m \sim 1000$ mL/g	0.7784 (Cs)	0.0546 (Cs)	92.99 (Cs)	1.33×10^4 (Cs)
		6.32 (Ca)	5.12 (Ca)	18.99 (Ca)	2.34×10^2 (Ca)
		4.76 (Mg)	3.84 (Mg)	19.33 (Mg)	2.40×10^2 (Mg)
		6.30 (Na)	5.22 (Na)	17.14 (Na)	2.07×10^2 (Na)
		3.60 (K)	2.28 (K)	36.67 (K)	5.79×10^2 (K)
	$V/m \sim 200$ mL/g	1.862 (Cs)	0.1204 (Cs)	93.53 (Cs)	2.89×10^3 (Cs)
		9.18 (Ca)	6.7 (Ca)	27.02 (Ca)	74.03 (Ca)
		9.3 (Mg)	6.38 (Mg)	31.40 (Mg)	91.54 (Mg)
		17.12 (Na)	15.9 (Na)	7.13 (Na)	15.35 (Na)
$V/m \sim 100$ mL/g	89.6 (K)	34 (K)	62.05 (K)	3.27×10^2 (K)	
	1.862 (Cs)	0.0666 (Cs)	96.42 (Cs)	2.70×10^3 (Cs)	
	9.18 (Ca)	5.32 (Ca)	42.05 (Ca)	72.56 (Ca)	
	9.3 (Mg)	5.88 (Mg)	36.77 (Mg)	58.16 (Mg)	
$\text{Sr}^{2+} + \text{Ca}^{2+} + \text{Mg}^{2+} + \text{Na}^+ + \text{K}^+$	$V/m \sim 200$ mL/g	17.12 (Na)	14.3 (Na)	16.47 (Na)	19.72 (Na)
		89.6 (K)	25.8 (K)	71.21 (K)	2.47×10^2 (K)
		1.24 (Sr)	0.1386 (Sr)	88.82 (Sr)	7.95×10^3 (Sr)
		5.02 (Ca)	2.5 (Ca)	50.20 (Ca)	1.01×10^3 (Ca)
		5.62 (Mg)	3.42 (Mg)	39.15 (Mg)	6.43×10^2 (Mg)
	$V/m \sim 100$ mL/g	12.52 (Na)	8.86 (Na)	29.33 (Na)	4.13×10^2 (Na)
		4.08 (K)	0.76 (K)	81.37 (K)	4.37×10^3 (K)
		1.24 (Sr)	0.0762 (Sr)	93.85 (Sr)	1.53×10^4 (Sr)
		5.02 (Ca)	2.28 (Ca)	54.58 (Ca)	1.20×10^3 (Ca)
$V/m \sim 100$ mL/g	5.62 (Mg)	2.88 (Mg)	48.75 (Mg)	9.51×10^2 (Mg)	
	12.52 (Na)	7.52 (Na)	39.94 (Na)	6.65×10^2 (Na)	
	4.08 (K)	0.58 (K)	85.78 (K)	6.03×10^3 (K)	

Table S16. The results of the ion exchange for FJSM-InMOF in the individual condition and coexistence of Cs⁺ and Sr²⁺ ($V/m = 1000$ mL/g).

Competing cation	Cs	Sr	Sr/Cs
Mass ratio			0.88
Sr (ppb) C_0		1240	1140
Sr (ppb) C_e		3	1.2
% Sr Removal		99.76	99.89
K_d^{Sr} (mL/g)		4.12×10^5	9.49×10^5
Cs (ppb) C_0	679.6		1176
Cs (ppb) C_e	12.4		16.6
% Cs Removal	98.18		98.59
K_d^{Cs} (mL/g)	5.38×10^4		6.98×10^4

Table S17. The comparison of Cs⁺ and Sr²⁺ removal efficiencies by various sorbents in this work and references.

Type of sorbents	Materials	Cs capacity, q_m (mg/g)	Relative amount of Cs removed (%)	residual Cs ⁺ concentration (ppb)	K_d^{Cs} (mL/g)	Sr capacity, q_m (mg/g)	Relative amount of Sr removed (%)	residual Sr ²⁺ concentration (ppb)	K_d^{Sr} (mL/g)
MOFs	FJSM-InMOF (this work)	198.63	99.63	2.6	7.50×10^4	43.83	99.89	1.2	9.49×10^5
	[(CH ₃) ₂ NH ₂][UO ₂ (L ₂)]·0.5DMF·15H ₂ O (H ₃ L=3,5-di(4'-carboxylphenyl) benzoic acid) ¹	about 145	94.51	50	7.55×10^3				
	MIL-101-SO ₃ H ²			890					2.29×10^4
	HKUST-1/KNiFC ³	153			1.5×10^3				
Commercial scavengers	AMP-PAN ^{4,5}	81			$\geq 10^2$	15			$\geq 10^2$
	TAM-5 ^{6,7}	191.8			$\geq 10^3$				
metal chalcogenides	FJSM-SnS ⁸	408.91	96-99%		2.36×10^3	65.19	Close to 100%		8.89×10^4
	KMS-1 ^{9,10}	226	98.9	11.4	2.1×10^4	77	99.89	10	4.50×10^5
	KMS-2 ¹¹	531.74			1.52×10^4	86.89			1.49×10^5
	KTS-3 ¹²	226	More than 97%		5.5×10^4	102	More than 98%		3.9×10^5
	K@RWY ¹³	310	~98%		$\geq 10^5$				
	GeSbS-2 ¹⁴	230.91			5.46×10^3				

In Table S17:

- (1) K_d^{Sr} of 9.49×10^5 mL/g is the highest for Sr²⁺ adsorption among Sr²⁺ scavengers.
- (2) The residual Sr²⁺ and Cs⁺ concentrations in the solution were 1.2 and 2.6 ppb, respectively, which are at a very low level.
- (3) About 99.9% of Sr²⁺ and 99.6% of Cs²⁺ could be removed by FJSM-InMOF which are comparable to those of the best scavengers for Sr²⁺ and Cs⁺, respectively.
- (4) The Cs⁺ exchange capacity of 198.6 mg/g is higher than those of the commercial AMP-PAN (81 mg/g) and TAM-5 (191.8 mg/g) which are currently marketed

by UOP as IONSIV IE-910 and IE-911, respectively. It also exceeds those of limited MOF examples such as magnetization of HKUST-1/KNiFC nanoparticles (153 mg/g; HKUST-1 = $[\text{Cu}_3(\text{BTC})_2]$; BTC = 1,3,5-benzenetricarboxylate; KNiFC = potassium nickel hexacyanoferrate) and $[(\text{CH}_3)_2\text{NH}_2][\text{UO}_2(\text{L}_2)] \cdot 0.5\text{DMF} \cdot 15\text{H}_2\text{O}$ (about 145 mg/g; H_3L_2 = 3,5-di(4'-carboxylphenyl)benzoic acid). The Sr^{2+} exchange capacity of 43.8 mg/g is about 3 times that of the commercial AMP-PAN (15 mg/g).

7. The elution

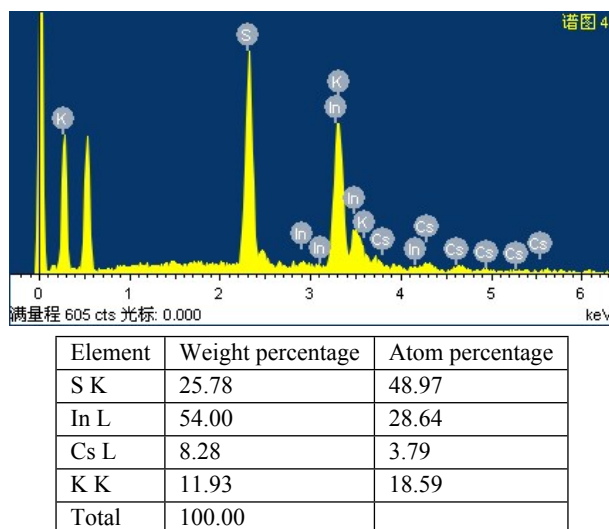


Figure S19. The EDS diagram and data for Cs⁺-exchanged products after eluted with saturated KCl methanol solution. The results show the ratio of K : Cs = 4.91 : 1 which verifies that nearly 83% Cs⁺ can be eluted by the cost-affordable and environmentally friendly method. ($V : m = 2000 \text{ mL g}^{-1}$, contact time 4 days, room temperature $\sim 25^\circ\text{C}$, and initial K⁺ concentration about 1300 ppm).

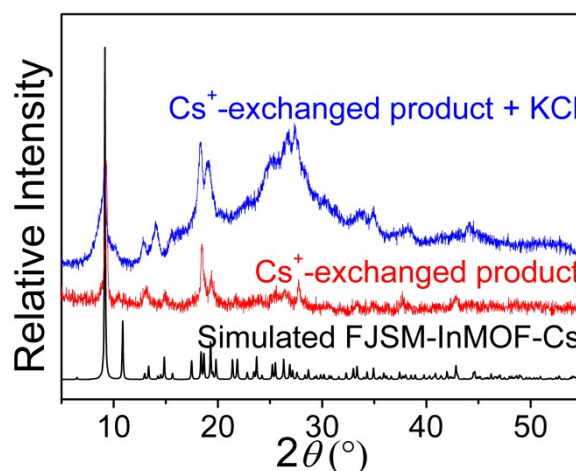


Figure S20. PXRD patterns of simulated FJSM-InMOF-Cs, Cs⁺-exchanged products and eluted products.

8. The studies on the stability of FJSM-InMOF

To assess the stability of FJSM-InMOF in various solvents, the crystals of FJSM-InMOF were immersed in different solvents for 24 h. The PXRD patterns reveal that the main framework structure of FJSM-InMOF could maintain in various solvents (Figure S21a). However, there is a phenomenon of crystal-to-crystal structural transformation for FJSM-InMOF with the change of space group from *Pccn* to *P4₁22* after FJSM-InMOF was immersed in CH₃CH₂OH, CH₃OH, DMF or DEF solutions, which could be revealed by the disappearance of (110) and (242) reflection peaks (Figure S21a) of crystalline FJSM-InMOF. While the framework of structure after transformation is similar to that of FJSM-InMOF-Cs (Figure S21b).

The stability of FJSM-InMOF in water has also been evaluated. As shown in Figure S22, FJSM-InMOF did not significantly change its crystalline structure after immersed in water at various pH values (in the range from 2.2 to 11.6) for 2 h. But the structure could not maintain in water for longer time. In fact, after treated with water for 24 h, FJSM-InMOF gradually transformed to another known compound, namely $\{[\text{In}(\text{TDC})(\text{OH})(\text{H}_2\text{O})]\}_n$,¹⁵ which possesses a neutral two-dimensional layered structure (Figure S23a).

To improve the water-stability of FJSM-InMOF, then we attempted to coat the polydimethylsiloxane (PDMS) on the FJSM-InMOF using the reported method, which has proved to be an efficient method to improve the water-stability of MOFs.^{16, 17} As shown in Figure S24, after coated with PDMS (the sample is denoted as FJSM-InMOF@PDMS), the sample exhibited obvious hydrophobic character compared with the pristine FJSM-InMOF while the framework of structure still maintained with a transformation of space group from *Pccn* to *P4₁22*. Impressively, the FJSM-InMOF@PDMS sample has outstanding water stability even after treated with water for 24 h (Figure S23b). Deeply systematic research on the removal of radioactive Cs^+ and Sr^{2+} ions by FJSM-InMOF@PDMS will be explored in the future.

Coating method: The PDMS coating of FJSM-InMOF was carried out by a vapor deposition technique which has been reported before.^{16, 17} A certain amount of FJSM-InMOF powders and PDMS stamp were placed on two glass dishes, respectively. The two dishes were placed in a sealed glass container, heated up by the speed of 1 °C/min, maintained at 235 °C for 4 h and then cooled to room temperature.

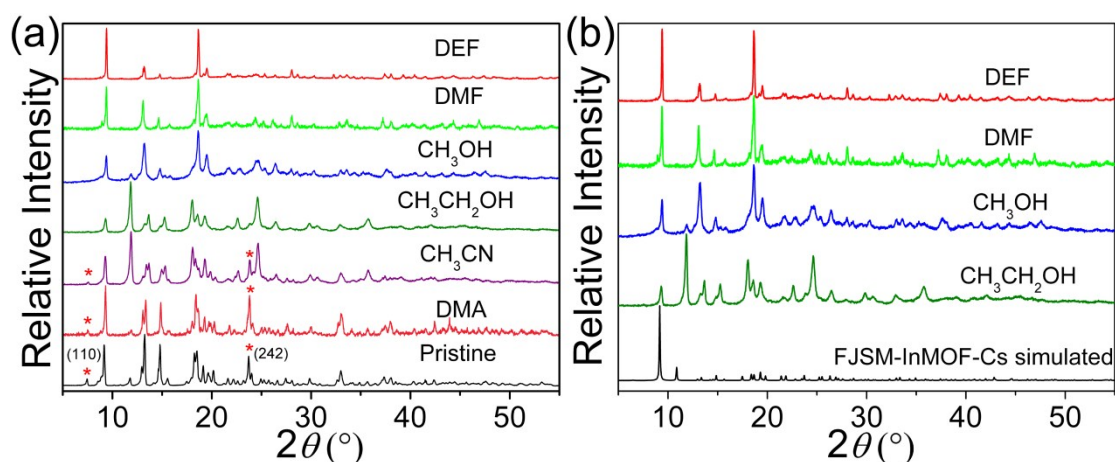


Figure S21. (a) XRD patterns for the FJSM-InMOF crystals after immersed in different solvents for 24 h. The (110) and (242) reflection peaks of pristine FJSM-InMOF maintained after immersed in DMA or CH₃CN but disappeared after immersed in CH₃CH₂OH, CH₃OH, DMF or DEF. (b) XRD patterns of FJSM-InMOF crystal products after immersed in CH₃CH₂OH, CH₃OH, DMF or DEF for 24 h, compared to the simulated one of FJSM-InMOF-Cs.

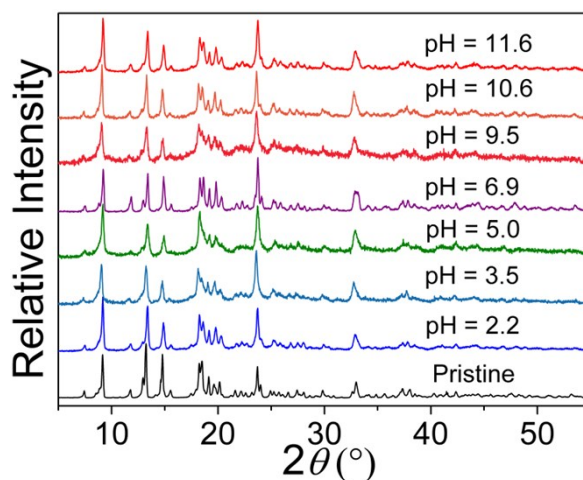


Figure S22. PXRD patterns of FJSM-InMOF crystals after immersed in water under various initial pH values for 2 h compared to that of the pristine.

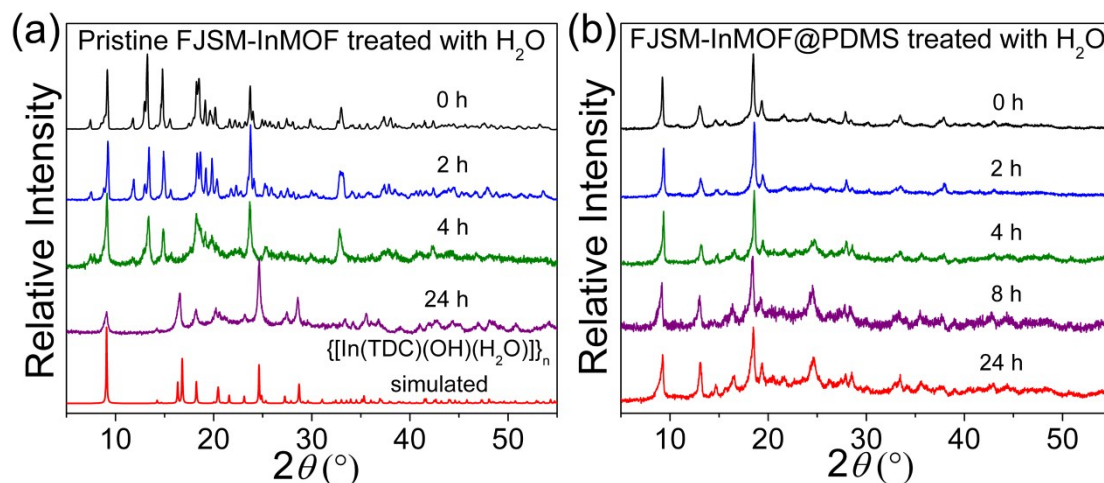


Figure S23. (a) PXRD patterns of FJSM-InMOF crystals after immersed in water for different times compared to the simulated one of $\{[\text{In}(\text{TDC})(\text{OH})(\text{H}_2\text{O})]\}_n$ ¹⁵. (b) PXRD patterns of FJSM-InMOF@PDMS after immersed in water for different times.



Figure S24. Photographs of FJSM-InMOF (a) and FJSM-InMOF@PDMS (b) after a drop of water was placed onto the samples. (c) PXRD patterns of the pristine FJSM-InMOF (bottom) and FJSM-InMOF@PDMS (top). The disappearance of (110) and (242) reflection peaks indicates the structural transformation after the coating process.

References

1. Y. L. Wang, Z. Y. Liu, Y. X. Li, Z. L. Bai, W. Liu, Y. X. Wang, X. M. Xu, C. L. Xiao, D. P. Sheng, J. Diwu, J. Su, Z. F. Chai, T. E. Albrecht-Schmitt, S. A. Wang, *J. Am. Chem. Soc.* **2015**, *137*, 6144-6147.
2. B. Aguila, D. Banerjee, Z. M. Nie, Y. Shin, S. Q. Ma, P. K. Thallapally, *Chem. Commun.* **2016**, *52*, 5940-5942.
3. S. Naeimi, H. Faghihian, *Sep. Purif. Technol.* **2017**, *175*, 255-265.
4. Y. Park, Y. C. Lee, W. S. Shin, S. J. Choi, *Chem. Eng. J.* **2010**, *162*, 685-695.
5. T. J. Tranter, R. S. Herbst, T. A. Todd, A. L. Olson, H. B. Eldredge, *Adv. Environ. Res.* **2002**, *6*, 107-121.
6. M. E. Huckman, I. M. Latheef, R. G. Anthony, *Sep. Sci. Technol.* **1999**, *34*, 1145-1166
7. Z. Zheng, C. V. Philip, R. G. Anthony, J. L. Krumhansl, D. E. Trudell, J. E. Miller, *Ind. Eng. Chem. Res.* **1996**, *35*, 4246-4256.
8. X. H. Qi, K. Z. Du, M. L. Feng, J. R. Li, C. F. Du, B. Zhang, X. Y. Huang, *J. Mater. Chem. A* **2015**, *3*, 5665-5673.
9. M. J. Manos, M. G. Kanatzidis, *J. Am. Chem. Soc.* **2009**, *131*, 6599-6607.
10. M. J. Manos, N. Ding, M. G. Kanatzidis, *Proc Natl. Acad. Sci. U.S.A.* **2008**, *105*, 3696-3699.
11. J. L. Mertz, Z. H. Fard, C. D. Malliakas, M. J. Manos, M. G. Kanatzidis, *Chem. Mater.* **2013**, *25*, 2116-2127.
12. D. Sarma, C. D. Malliakas, K. S. Subrahmanyam, S. M. Islama, M. G. Kanatzidis, *Chem. Sci.* **2016**, *7*, 1121-1132.
13. H. J. Yang, M. Luo, L. Luo, H. X. Wang, D. D. Hu, J. Lin, X. Wang, Y. L. Wang, S. A. Wang, X. H. Bu, P. Y. Feng, T. Wu, *Chem. Mater.* **2016**, *28*, 8774-8780.
14. B. Zhang, M. L. Feng, H. H. Cui, C. F. Du, X. H. Qi, N. N. Shen, X. Y. Huang, *Inorg. Chem.* **2015**, *54*, 8474-8481.
15. Z. Chen, Y. Zuo, X. H. Li, H. Wang, B. Zhao, W. Shi, P. Cheng, *J. Mol. Struct.* **2008**, *888*, 360-365.
16. Yuan, X. Liu, O. Akbulut, J. Hu, S. L. Suib, J. Kong, F. Stellacci, *Nat. Nanotechnol.* **2008**, *3*, 332-336.
17. W. Zhang, Y. Hu, J. Ge, H. L. Jiang, S.-H. Yu, *J. Am. Chem. Soc.* **2014**, *136*, 16978-16981.